Large-signal time-domain modeling of low-pressure rf glow discharges

Michael S. Barnes, Tina J. Colter, and Michael E. Elta
Department of Electrical Engineering and Computer Science, Solid-State Electronics Laboratory, The University of Michigan, Ann Arbor, Michigan 48109

(Received 9 June 1986; accepted for publication 18 September 1986)

Large-signal time-domain modeling (simulation) of rf glow discharges is a very useful and potentially accurate tool for the study of low-pressure (50–500-mT) gaseous electronics at high frequencies. Unfortunately, the computational limitations imposed for stability, accuracy, and efficiency can often hinder the production of useful, cost-effective results. This paper describes a self-consistent argon rf glow-discharge simulation at 13.56 MHz for equal- and unequal-area parallel-plate electrode geometries. Some of the numerical problems associated with this type of simulation are identified and the numerical methods used to overcome them are described. To illustrate the usefulness of this modeling scheme, the plasma potential and the cathode dc bias are examined as functions of electrode area ratio and rf power.

I. INTRODUCTION

rf glow discharges at 13.56 MHz are fundamental components of many integrated circuit fabrication processes. In particular, for plasma etching of thin films,[1] a molecular rf glow discharge (often with a multicomponent gas mixture) is used to generate chemically reactive species. This process is often assisted by (reactive) ion bombardment of the etch substrate resulting from electrode sheath formation. Similarly, inert rf glow discharges with unequal-area electrode geometries are frequently used in sputter deposition and sputter etching[2] where very high ion bombardment energies are required.

The large-signal behavior of a rf glow discharge is attributed to highly nonlinear carrier dynamics, electrode sheath effects, and interaction with an external circuit. The aim of the simulation work described in this paper is to self-consistently solve the one-dimensional forms of the electron and ion continuity equations and Poisson's equation for argon rf glow discharges at 13.56 MHz (see Figure 1), subject to boundary conditions which include the effect of any external circuit. Using standard notation and sign convention, the equations are

$$\frac{\partial n}{\partial t} = \frac{1}{q}\frac{\partial J_n}{\partial x} + G - L, \tag{1}$$

$$\frac{\partial p}{\partial t} = -\frac{1}{q}\frac{\partial J_p}{\partial x} + G - L, \tag{2}$$

and

$$\frac{\partial E}{\partial x} = \frac{q}{\epsilon}(p - n). \tag{3}$$

In (1)–(3), n is the electron number density, p the ion number density, E the electric field, G the generation rate, and L the loss rate. J_n and J_p represent the electron and ion current densities, respectively, q is the electronic charge, and ϵ the permittivity (of free space in this case). Manipulation of (1)–(3) leads to spatial conservation of total current:

$$\frac{\partial}{\partial x}\left(\epsilon\frac{\partial E}{\partial t} + J_n + J_p\right) = 0. \tag{4}$$

The mathematical problem is therefore defined by any three of (1)–(4) when boundary and initial conditions are known. The initial conditions include the values of electric field and carrier densities as functions of distance at $t = 0$. Three independent sets of boundary conditions on E, n, p or some dependent variables must be specified for time advancement.

The particle current densities J_n and J_p are assumed to consist of a drift term and a diffusion term. The drift term is due to the force exerted on the particle by the electric field whereas the diffusion term describes particle motion due to concentration gradients:

$$J_n = -qnv_n(E) + q\frac{\partial}{\partial x}[nD_n(E)], \tag{5}$$

$$J_p = qpv_p(E) - q\frac{\partial}{\partial x}[pD_p(E)]. \tag{6}$$

In (5) and (6), v_n and v_p are the particle velocities and D_n and D_p are the particle diffusivities for electrons and ions respectively. Particle generation is assumed to be primarily due to electron-neutral impact ionizing collisions such that

$$G = \alpha|J_n|. \tag{7}$$

The standard form of α known as Townsend's first ionization coefficient[3] is given by

$$\alpha/P = A\exp[-(BP/E)], \tag{8}$$

where A and B are empirically determined constants. A rf glow discharge at 13.56 MHz is in the diffusion-controlled breakdown regime[4] which means that no electron emission from the electrodes is necessary to sustain the discharge. Therefore, insulated electrodes (typically found in plasma etch and rf sputter chambers) are considered in the self-consistent formulation. The dominant electron loss mechanism is electron-ion recombination on the electrode and chamber wall surfaces.

The remainder of the paper is organized as follows. Section II describes the use of Monte Carlo techniques for the calculation of transport coefficients for electrons and ions and Townsend's first ionization coefficient as a function of electric field. In Sec. III, the numerical implementation of (1)–(8) is discussed with the emphasis placed on boundary conditions, computational limitations, and the unequal area

 0021-8979/87/010081-09$02.40

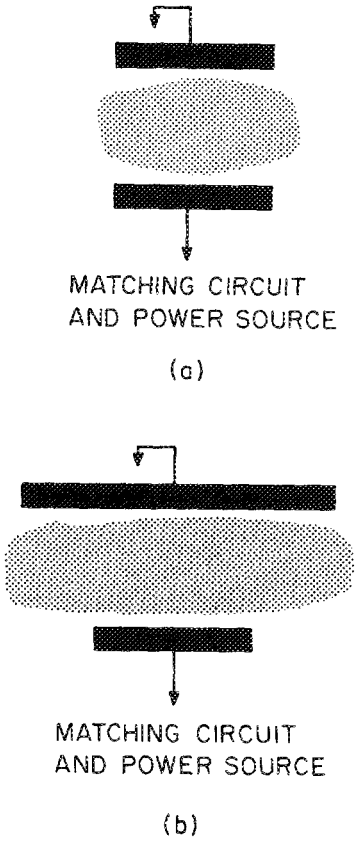

FIG. 1. Simulated rf glow discharge electrode configurations. (a) Equal-area electrodes. (b) Unequal-area electrodes.

electrode geometry factor. In Sec. IV, results from the argon rf glow discharge at 13.56 MHz are presented. Section V concludes with a summary and discussion concerning the usefulness of this type of modeling as part of an effort to enhance the theoretical understanding of integrated circuit fabrication processes in quantitative terms.

II. TRANSPORT AND RATE PARAMETERS

The development of transport and rate data sets as a function of the electric field is a fundamental component of rf glow discharge modeling since existing data is very limited. Experimental data[3–6] has been gathered at pressures typically an order of magnitude higher than those considered in this work. Although most of this data has been correlated to functions of electric field divided by pressure [i.e., $y = f(E/p)$], its validity is questionable at low pressures. To calculate drift velocities, diffusion coefficients, and ionization rates, the energy distribution function and the collision cross sections must be known. The rate and transport parameters can then be determined by averaging the quantity of interest α over the distribution function, i.e.,

$$\langle \alpha \rangle = n^{-1} \int_0^\infty \alpha f(u) du. \tag{9}$$

Several methods are available for computing the electron energy distribution function. These include spherical harmonic expansions of the Boltzmann transport equation,[7,8] two temperature energy balance schemes,[9–11] and Monte Carlo simulations of electron swarms.[12–14]

A very common technique used in semiconductor device modeling for developing rate and transport coefficient data sets is to perform a Monte Carlo simulation of a single charged particle in an infinite homogeneous medium under the influence of a static electric field.[15,16] In rf glow discharges, electron-neutral and ion-neutral collisions are the dominant energy and momentum transfer processes. This is simply because neutral concentrations are typically 4–6 orders of magnitude higher than electron and ion concentrations. In other words, the neutral medium appears homogeneous to electrons and ions regardless of the spatial charge distribution. Furthermore, since neither charged particle can traverse the discharge electrode separation distance during a rf cycle, the medium looks infinite for time scales on the order of a rf period.

In order to perform this type of Monte Carlo simulation, electron-neutral and ion-neutral collision cross sections must be known. From these, the individual scattering rates[17] are determined using

$$\Gamma_{xy} = C u^{1/2} P \sigma_{xy}(u), \tag{10}$$

where C is a constant related to particle mass, P is the chamber pressure, and u is the particle energy. Γ_{xy} and σ_{xy} are the scattering rate and total collision cross section for the process $x \rightarrow y$. Summing all scattering rates for a particle yields the maximum scattering rate $\Gamma_{\max}$ considered in the simulation. By including self-scattering,[18] the mean interarrival time (i.e., the mean time between collisions) is simply the inverse of $\Gamma_{\max}$. Using a uniform random number generator,[19] the flight duration times t_r can be determined from

$$t_r = -(1/\Gamma_{\max}) \ln(r), \tag{11}$$

where $r = \text{uni}[0,1]$. By generating another random variable with a uniform distribution between zero and $\Gamma_{\max}$, the type of scattering is selected.[20] Once the scattering mechanism has been determined, the particle state is updated (unless self-scattering occurs), and the process is repeated a large number of times.

Using B-state estimators[21] (i.e., sample the particle before each scattering event), the distribution functions, the average energies and the drift velocities can be calculated in a straightforward manner by recording the particle velocities and energy at t_r. Diffusion coefficients are calculated using characteristic energies and mobilities.[5] The characteristic energy for electrons is two-thirds the average electron energy and the mobilities are calculated by dividing the drift velocity by the electric field magnitude. Townsend's first ionization coefficient is calculated by counting the number of ionizing events, dividing by the total elapsed simulation time, and dividing this quantity by the drift velocity.[15]

For argon, the three dominant electron-neutral collisions are momentum transfer, excitation, and ionization. Data for these cross sections as a function of energy has been gathered from several sources.[5,22] Figure 2(a) illustrates electron transport data curves as a function of electric field at 300 mT. To produce these data curves, many individual Monte Carlo simulations must be run, each with a large number of samples to reduce the statistical variance. At low electric fields (e.g., 1–5 V/cm), calculated electron drift velocities are in fairly good agreement with experimental data.[5,6] Electron diffusivities and high field (e.g., 10–1000 V/cm) electron drift velocities have not been experimentally

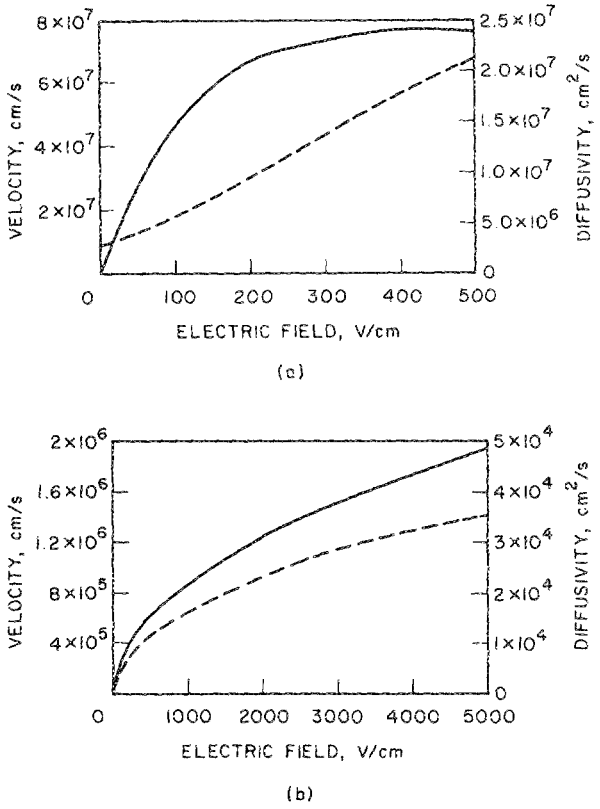

FIG. 2. Transport data from Monte Carlo simulations: (a) for electrons, (b) for ions. Solid lines indicate velocity and dashed lines indicate diffusivity.

determined at low pressures. The electron drift velocity demonstrates a square root dependence on the electric field.

The argon ion Monte Carlo simulation only considers hard sphere elastic scattering and self-scattering. If real scattering is chosen at the end of an ion flight, a neutral with three independent Gaussian distributed velocities is generated. Both the ion and neutral are transformed from laboratory coordinates to center-of-mass coordinates in three-dimensional velocity space. Radial and azimuthal scattering angles are generated with uniform distributions to determine the ion and neutral states after the collision. Typical ion transport data curves are illustrated in Fig. 2(b) as a function of the electric field at 300 mT. The ion drift velocity is on the same order of magnitude as that given by the experimental correlation of Frost.[23] (This correlation was fit to data at higher pressures.) Experimental ion diffusivity data has not been gathered at low pressures.

If relaxation time effects are assumed negligible, the transport and rate data gathered from simulated electrons and ions under static field conditions is valid at rf frequencies (i.e., the quasi-static approximation). Steady-state momentum and energy relaxation time calculations[24] indicate that relaxation time effects can be completely ignored for ions. The electron momentum relaxation times at 300 mT are much smaller than one rf period at 13.56 MHz (approximately 74 ns) for all electric field strengths in the large-signal simulation. This is expected since all collisions have been assumed to be momentum randomizing. On the other hand, the electron energy relaxation times are larger than the rf period for fields less than 10 V/cm. This effect occurs since the electrons must "heat" to an energy above the first inelastic threshold before they can undergo a significant energy loss during a collision. As a result, there will be some degree of velocity overshoot and undershoot in the low field regions of the rf glow discharge which cannot be properly modeled by the drift-diffusion–based formulation discussed in Sec. III.

III. LARGE-SIGNAL SIMULATION METHODS

A. The basic scheme

The rf glow discharge model consisting of (1)–(8) can only be solved when several implicit assumptions and idealizations have been made. These include neglecting fringing fields and currents, neglecting relaxation time effects, and the phenomenological treatment of electron impact ionization. Despite these approximations, the rf glow discharge model does produce valuable results for research purposes. Throughout this section, a familiarity with basic finite difference numerical methods[25,26] is assumed.

The basic large-signal time-domain simulation scheme uses a finite grid of points in space and time for the evaluation of the electric field and the carrier densities, subject to boundary conditions. Knowledge of these quantities at each time level enables the calculations of the terminal discharge voltage and current. When a steady-state solution has been reached, the voltage and current waveforms can be Fourier analyzed for discharge impedance and power calculations. In most cases it is numerically more efficient to reach a steady-state solution with a transient method rather than with a steady-flow approach.[26]

A very important criterion for simulations involving charged particles is that no artificial sourcing or sinking of particles occurs during advancement to the next time level. Upwind differencing of the drift terms in (1) and (2) using a staggered space grid (see Fig. 3) has been frequently employed for simulating semiconductor transit-time devices.[16,27,28] This method is an explicit transient numerical method which suffers from artificial diffusion.[26] Fortunately, the pseudodiffusion coefficient can be made much less than the physical diffusion coefficient and has very little effect on the results. The basic finite difference forms of (1) and (2) are

$$q\frac{n_j^{k+1}-n_j^k}{\Delta t}=\frac{JN_{i+1}^k-JN_i^k}{\Delta x}, \tag{12}$$

$$q\frac{p_j^{k+1}-p_j^k}{\Delta t}=-\frac{JP_{i+1}^k-JP_i^k}{\Delta x}, \tag{13}$$

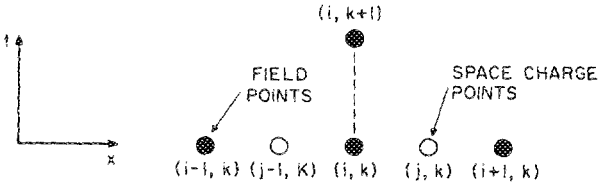

FIG. 3. Finite difference space-time diagram.

when the diffusion and the generation terms have been neglected (for simplicity in presentation). The superscript k refers to the time step and subscripts i and j refer to the space mesh as shown in Fig. 3. In (12) and (13) JN and JP are the drift current densities for electrons and ions, respectively, Δt is the timestep and Δx is the spacestep. The loss term due to ambipolar diffusion has been determined to have very little effect on the results of this simulation and can be omitted for numerical efficiency. (This term cannot be omitted from radial positive column energy balance calculations.[9–11]) The expressions for the drift currents using upwind differencing with the electric field $E_i^k \geqslant 0$ are

$$JN_i^k = -qn_j^k v_{ni}^k, \tag{14}$$

$$JP_i^k = qp_{j-1}^k v_{pi}^k. \tag{15}$$

For $E_i^k < 0$:

$$JN_i^k = -qn_{j-1}^k v_{ni}^k, \tag{16}$$

$$JP_i^k = qp_j^k v_{pi}^k. \tag{17}$$

All transport coefficients and Townsend's first ionization coefficient are stored in look-up tables for numerical efficiency.

The explicit treatment of physical diffusion suffers from Fourier overshoot of spatial modes.[16] As a result, a two-step time advancement method will be used to include physical diffusion. Upwind differencing will be used to explicitly calculate the drift terms in step 1 followed by an implicit calculation of the diffusion terms[16] in step 2. The continuity equations in finite difference notation are now given by

$$q\frac{n_j^{k+1}-n_j^k}{\Delta t} = G_j^k + \frac{JN_{i+1}^k - JN_i^k}{\Delta x} + \frac{JND_{i+1}^k - JND_i^k}{\Delta x}, \tag{18}$$

$$q\frac{p_j^{k+1}-p_j^k}{\Delta t} = G_j^k - \frac{JP_{i+1}^k - JP_i^k}{\Delta x} - \frac{JPD_{i+1}^k - JPD_i^k}{\Delta x}, \tag{19}$$

where the drift components are the same as (14)–(17) and the diffusion components are

$$JND_i^k = qD_{ni}^k \frac{n_j^{k+1} - n_{j-1}^{k+1}}{2\Delta x}, \tag{20}$$

$$JPD_i^k = -qD_{pi}^k \frac{p_j^{k+1} - p_{j-1}^{k+1}}{2\Delta x}. \tag{21}$$

D_n and D_p denote the diffusivities for electrons and ions, respectively. The generation term at the ith point is determined using Townsend's first ionization coefficient and the electron current magnitude:

$$G_i^k = \alpha_i^k |JN_i^k + JND_i^{k-1}|. \tag{22}$$

The generation term at the jth point is then simply

$$G_j^k = \tfrac{1}{2}(G_{i+1}^k + G_i^k). \tag{23}$$

The continuity equations are advanced to the next time level by incorporating the boundary conditions and performing a matrix inversion. Fortunately, the matrix is tridiagonal and can be solved very efficiently.[26]

B. The boundary conditions

For the correct solution of a system of partial differential equations, the boundary and initial conditions must be accurately specified. In particular, a numerical boundary condition must suitably describe the physical problem without introducing any numerical artifacts. For a one-dimensional argon rf glow discharge, three sets of independent boundary conditions on E, n, p or some dependent variables must be specified. The initial conditions at $t = 0$ include the values of electric field and carrier densities as functions of distance. In the interest of numerical efficiency, the initial carrier densities are set to a constant background level across the discharge resulting in an initial electric field of zero.

In the two-step explicit-implicit method outlined in Sec. III A, the electron and ion boundary conditions must be specified at each step. For the explicit calculation of the drift components using upwind differencing, the boundary current is set to zero if the particle velocity direction is away from the electrode. (It has been assumed that the electrodes are insulating and nonemitting.) The boundary condition on the diffusion component is set by assuming the carrier gradient at the electrode surface is zero. Boundary conditions of this form are considered to be mixed or Robbin's type.[26]

The boundary condition for Poisson's equation must include the effects of an external circuit as well as the temporally varying charge on the electrodes. The electric field at each grid point is calculated in a very straightforward manner using

$$E_{i+1}^k = E_i^k + \frac{q\Delta x}{\epsilon_0}(p_j^k - n_j^k). \tag{24}$$

This relationship only determines the relative electric field values at each point. The absolute field levels are set by the boundary conditions. The value of the charge on each electrode is stored at each timestep. This permits the field to be determined in the insulating coating by using the relationship between the surface charge and the normal electric fields

$$\epsilon_d E_d - \epsilon_0 E = \rho_s, \tag{25}$$

where ρ_s is the surface charge density (and subscript d refers to the insulated electrode coating).[29] The absolute field level is then set by incorporating the effects of an external circuit. The equivalent circuit of a rf power source and matching network can be represented by the tank circuit in Fig. 4 when it is assumed that an optimum match has been achieved. The

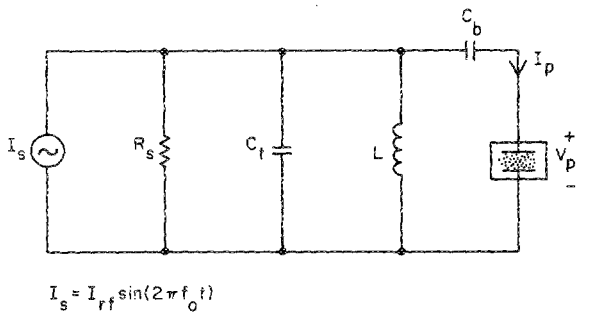

FIG. 4. External equivalent circuit for boundary condition.

values of the inductor and capacitor are determined so that the tank is resonant at 13.56 MHz. The field is integrated across the discharge at each timestep to determine the instantaneous rf voltage. The total discharge current is calculated using

$$I_{\rm tot}(t)=\frac{1}{W}\int_0^W\left(J_N+J_P+\epsilon\frac{\partial E}{\partial t}\right)dx \tag{26}$$

in order to determine the true discharge voltage from the external circuit. The field in the discharge is then adjusted so that the instantaneous voltage is equal to the true voltage.

C. The geometry factor

For equal-area electrode geometries, Gauss's law is satisfied by neglecting fringing fields and currents in the one-dimensional rf glow discharge model. In other words, it is assumed that all current and electric field fluxes are normal to the electrodes for the cylindrical parallel plate geometry. For the inverted conic frustrum geometry of the unequal area electrode configuration [see Fig. 5(a)], a one-dimensional model may still be useful by introducing a geometry area factor $b(x)$[30] and neglecting fringing fields and currents. The computational error introduced by these assumptions can be minimized by not allowing $b(x)$ to vary by large amounts over a space step. By assuming that (a) there is no current flow at the edges of the small volume element of length Δx in Fig. 5(b) and that (b) all field flux out of a volume element enters the next volume element (except at the electrodes), the two-dimensional forms of Poisson's equation and the electron continuity equation can be written as

$$\frac{\partial[b(x)E(x,t)]}{\partial x}=\frac{q}{\epsilon_0}[b(x)p(x,t)-b(x)n(x,t)] \tag{27}$$

and

$$\frac{\partial[b(x)n(x,t)]}{\partial x}=\frac{1}{q}\frac{\partial[b(x)J_n(x,t)]}{\partial x}+b(x)G(x,t). \tag{28}$$

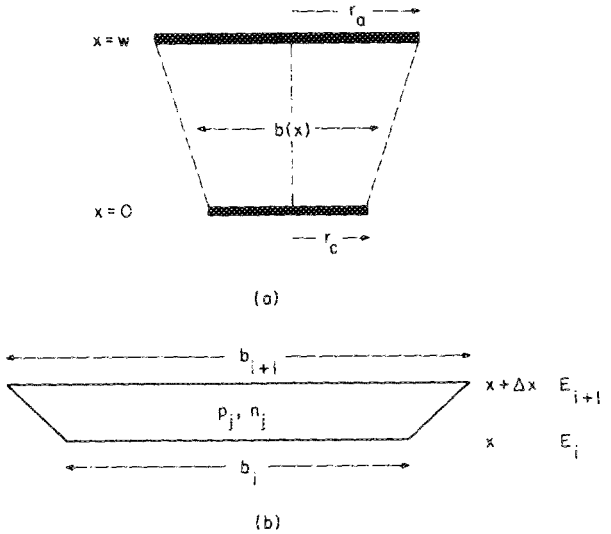

FIG. 5. Unequal-area geometry factor (a) as a function of distance and (b) for a discrete volume element.

D. Computational limitations

Several limitations on timestep and spacestep size result from stability problems of the numerical methods used to solve (1)–(3). A fundamental limitation on all explicit time advancement numerical methods is the Courant–Friedrich's–Lewy condition[31]

$$c=\frac{v_{\max}\Delta t}{\Delta x}\leqslant 1. \tag{29}$$

This condition prevents a particle from advancing more than one grid point per timestep. The maximum diffusion coefficient (divided by the spacestep) is omitted from this expression since the diffusion components of the continuity equations are solved implicitly. Since this is a fluid flow problem, a Reynold's number restriction on the spacestep[26] must be satisfied to ensure no zero overshoot of the carrier densities. The pseudodiffusion from the upwind differencing automatically satisfies this limitation.

Another limitation on the timestep arises as a result of the space-charge stability condition and the field stability condition. A space-charge instability usually occurs when the electric field is low, the particle densities are high, and the space charge is almost neutral and uniform.[32] When solving the continuity equations numerically it is assumed that the rate of change of net charge is constant and follows the tangent line of an exponential curve. To prevent the net charge from having the wrong sign, the timestep must be limited by

$$\Delta t\leqslant\frac{\epsilon_0}{q(\mu_n n+\mu_p p)}, \tag{30}$$

where μ_n and μ_p are the electron and ion mobilities, respectively. The quantity on the right-hand side of (30) is the dielectric relaxation time. Similarly, a field instability usually occurs at a location where there is a large particle density gradient, such as the gradients found in the electrode sheath.[32] When this instability occurs, the net space charge accumulated during Δt will be so large as to make E overshoot its true value. Oscillations will then develop in subsequent timesteps as a result. The timestep limitation due to the field instability condition is also given by (30).

IV. LARGE-SIGNAL SIMULATION RESULTS

Before large-signal results can be obtained, the external equivalent circuit values and the discharge parameters must be specified. The circuit values must be chosen to physically model the matching circuit and power supply and more importantly numerically stabilize the self-consistent solution. The parallel tank circuit illustrated in Fig. 4 is resonant at 13.56 MHz when the tank capacitance C_t and the blocking capacitance C_b are set to 100 pF and the inductance L to 1.378 μH. Other combinations of L, C_t, and C_b are possible but numerical stability and computational efficiency are sacrificed to some degree. The source resistance R_s is set to 1 MΩ and the source current amplitude is set to 1.2 A for the simulated results in Figs. 6 and 7. The electrodes are assumed to be coated with a 100-μm layer of an oxide (with a relative dielectric coefficient of 4.0). The cathode radius is

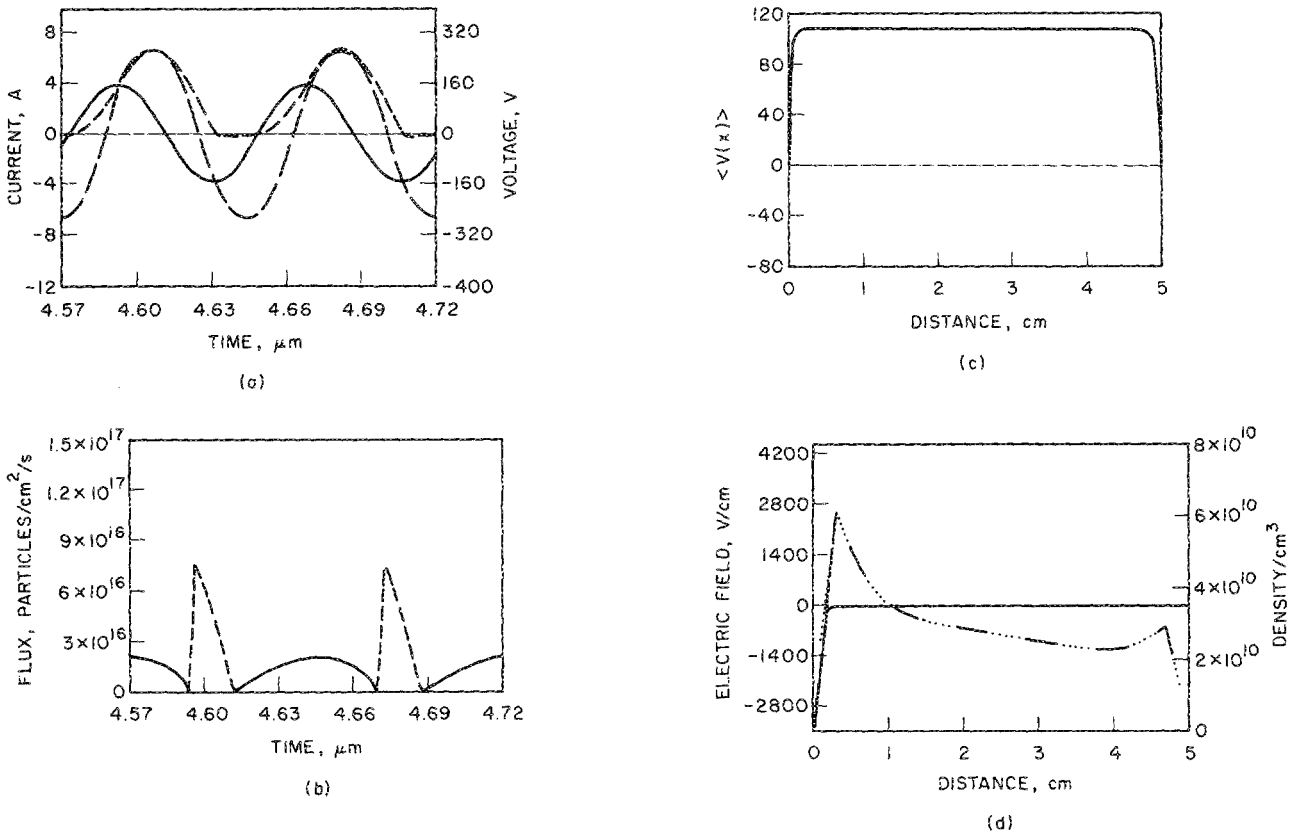

FIG. 6. Results from large-signal simulation for an equal-area electrode configuration. (a) Steady-state current and voltage waveforms. The solid line indicates the terminal current, the large dashed line the terminal voltage, and the small dashed line the plasma potential. (b) Steady-state cathode particle fluxes. The solid line indicates the ion flux and the dashed line the electron flux. (c) Time-averaged spatial voltage distribution. (d) Instantaneous electric field and carrier density profiles. The solid line indicates the electric field, the dashed line the electron density, and the dotted line the ion density.

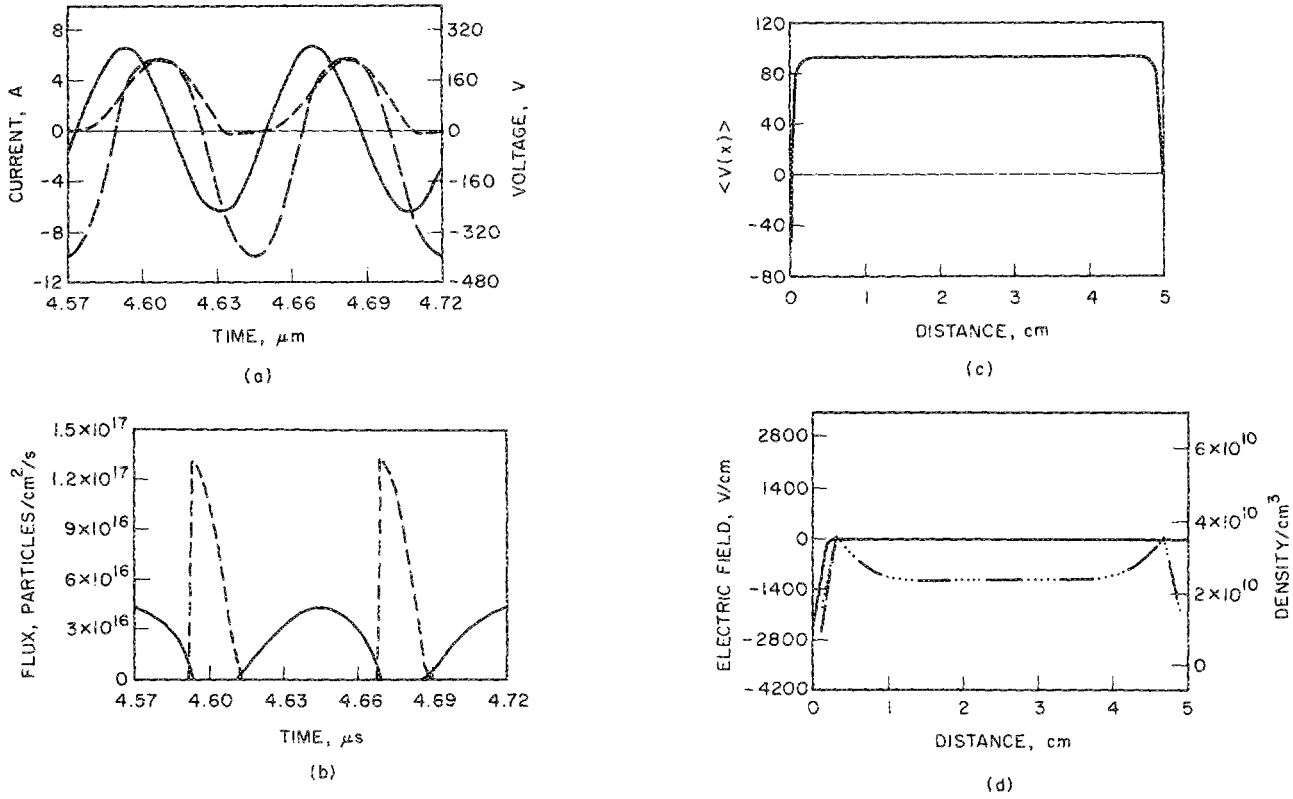

FIG. 7. Results from large-signal simulation for unequal area electrode configuration. The legends used in these figures are the same as those used in Fig. 6. (a) Steady-state current and voltage waveforms. (b) Steady-state cathode particle fluxes. (c) Time-averaged spatial voltage distribution. (d) Instantaneous electric field and carrier density profiles.

10 cm, the electrode separation is 5 cm, and the operating pressure is 300 mT.

The steady-state criterion for the self-consistent rf glow-discharge simulation are twofold. First, the voltage and current waveforms are Fourier analyzed every two rf cycles. The rf power and impedance are then calculated at the fundamental (i.e., 13.56 MHz) and checked against the values from the previous two rf cycles. When the percent differences in these quantities are below a specified value, a second criterion, the net charge impinging on the cathode, is imposed. When the number of electrons and ions striking the cathode during two consecutive rf cycles differ by less than a specified percentage, a steady state is assumed to have been reached. For the results presented below, the impedance criterion is assumed to be satisfied when the percent differences are less than 5% and the net charge criterion when the percent difference is less than 1%.

Results from the large-signal simulation are presented in Figs. 6(a)–6(d) for an equal area (1:1 plate ratio) rf glow discharge. Figure 6(a) illlustrates the discharge terminal current and voltage waveforms over two rf cycles. These waveforms appear to have similar shapes to those recorded experimentally.[33] Also included in this plot is the time-varying plasma potential. Figure 6(b) depicts the electron and ion fluxes to cathode over two rf cycles. Careful observation shows that the number of electrons and ions striking the cathode during a rf period are (approximately) equal. This trend has been predicted by several researchers.[2,4,34,35] Figure 6(c) illustrates the spatial voltage distribution time-averaged over a rf cycle. The plasma potential V_p will be fined as the midpoint value of this voltage distribution for the remainder of this paper. Figure 6(d) depicts the instantaneous spatial electric field and carrier density profiles at the end of the last timestep in the simulation. This corresponds to the last point in time shown in Figs. 6(a) and 6(b). Figures 7(a)–7(d) illustrate results from a 2:1 (unequal) area ratio discharge. The shapes of the time-averaged spatial voltage distribution in Figs. 6(c) and 7(c) are similar to those sketched in Ref. 1. Furthermore, the degree of ionization is approximately 10^{-6} and the electron/ion concentration in the plasma region is on the order of magnitude of 10^{10} cm^{-3} as suggested in Refs. 2 and 36. The shapes of the electron concentration profiles are similar to the time-averaged spatial emission measurements in Ref. 37. (The rate of excitation is proportional to the electron density.[9])

By fixing all but one of the input parameters, the characteristics of a rf glow discharge can be studied as a function of plate separation, operating frequency, electrode area ratio, and pressure. By selecting different values of input rf current I_{rf}, the simulated operating point can be varied once the geometry and circuit parameters have been fixed. This facilitates the study of a rf glow discharge as a function of rf power. As an example of the usefulness of this type of simulation, the plasma potential V_p and the magnitude of the cathode dc bias V_{dc} are plotted in Fig. 8 as functions of real rf power for different electrode area ratios. Although there is no existing experimental data at 300 mT to compare these results to, the trends have been experimentally verified by many researchers.[2,34,35,38] That is, the plasma potential increases with rf power and decreases as the electrode area ratio is increased. Moreover, the cathode dc bias increases as the electrode area ratio and rf power are increased (except for the equal areas case where no dc bias is observed).

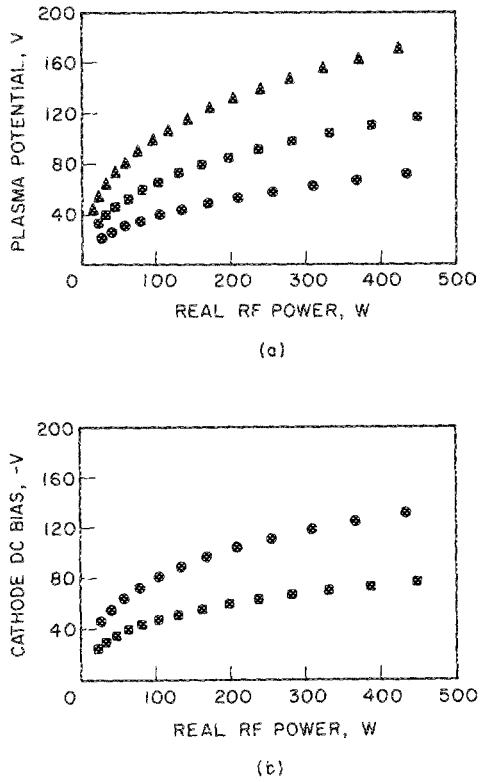

FIG. 8. Large-signal simulation output parameters as a function of real rf power. (a) Plasma potential vs real rf power. (b) Cathode self-bias vs real rf power. Triangles (▲) indicate 1:1 area ratio, squares (■) 2:1 area ratio, and circles (●) 4:1 area ratio.

The timestep advancement of this simulation is performed in a multistep manner to facilitate computational efficiency as well as satisfy the stability criterion (29) and (30). The Courant condition (29) is automatically satisfied at 300 mT by setting the "global" timestep to the rf period divided by 64. On the other hand, the space-charge and field stability limitations (30) can be several orders of magnitude less than the "global" timestep. Therefore, at the beginning of each timestep, the condition (30) is computed and the "global" timestep is subdivided if necessary. The execution time for the simulated data in Fig. 8 ranged from about 40 cpu s to about 120 cpu s on an Amdahl 580 series 5860 mainframe. The execution time was observed to increase as the rf power and electrode area ratio were increased due to the stability condition (30).

V. CONCLUDING REMARKS

The motivation for the development of the computer simulation described in this paper has its basis in the need to quantitatively understand microelectronic plasma processing. The authors of this paper believe that if the time-averaged ion and free radical fluxes to the thin-film or semiconductor substrate can be predicted with a reasonable degree of accuracy, a great deal of information concerning the surface

chemical mechanisms (of plasma processing) can be deduced. It must be realized that numerical efficiency prohibits running the simulation for time scales on the order of plasma processing times. Typically, a rf glow-discharge steady-state solution is reached for characteristic times on the order of several microseconds. Therefore, even with present state-of-the-art computing facilities, it is unlikely that a rf plasma chemical process can be completely simulated in time.

The Monte Carlo methods described in this paper were developed due to the limited availability of the transport and rate data for electrons and ions in molecular gases. Although these methods have not yet been extended to molecular gases, it is believed that if these methods verify existing experimental data for an inert gas such as argon reasonably well, they will provide a reasonable estimate of the transport and rate data for molecular gases. Future Monte Carlo work includes extending the simulation to handle molecular gases and incorporating charge exchange in the ion Monte Carlo simulation.

The large-signal time domain model and the continuum model[39] are believed to represent the state-of-the art in modeling of rf glow discharges in the diffusion-controlled breakdown regime. This scheme has the advantage over the continuum model in that it is a time-evolved solution subject to boundary conditions which take into account the charging and discharging of insulated electrodes and the effects of any external circuit. The program is designed in a modular fashion to facilitate the investigation of the effects of a more complex external circuit and different electrode boundary conditions (e.g., electron emitting electrodes). Moreover, unequal-area electrode effects including the development of a dc self-bias can be investigated with the large-signal model. The large-signal model suffers from the disadvantage that a spatial energy balance is not taken into account (i.e., the drift-diffusion approximation has been used). On the other hand, the continuum model assumes a constant electron mobility, diffusivity, and ionization coefficient which effectively decouples the energy balance equation from the self-consistent solution. As a result, the large-signal model, using field-dependent nonlinear electron rate and transport coefficients (determined using Monte Carlo methods), more suitably models the highly nonlinear carrier dynamics. Nevertheless, both models implicitly assume that the electron transport phenomena are in equilibrium with the electric field and therefore do not properly model electron heating effects in the low field regions of the rf glow discharge. These nonequilibrium phenomena can be sufficiently accounted for using a self-consistent formulation including the first and second moments of the Boltzmann transport equation (provided that ballistic electron transport can be ignored).

The authors plan to further investigate the effectiveness of this type of modeling by attempting to extend the model to consider complex molecular gas sets typically used in plasma processing. This appears to involve developing rate and transport data sets as a function of electric field for these gases and identifying the important species for a particular plasma process. Uncharged free radical species can be included if rate and diffusion coefficients are known or calculated. Since the usefulness of any model lies in its ability to accurately predict observed experimental phenomena, experimental methods to verify predicted results from the large-signal model are also being investigated.

ACKNOWLEDGMENT

This work is being sponsored by the Semiconductor Research Corporation under Contract No. 84-01-045.

[1]J. W. Coburn, *Plasma Etching and Reactive Ion Etching*, American Vacuum Society Monograph Series (American Institute of Physics, New York, 1982).
[2]B. N. Chapman, *Glow Discharge Processes* (Wiley, New York, 1980).
[3]J. D. Cobine, *Gaseous Conductors* (McGraw-Hill, New York, 1941).
[4]E. Nasser, *Fundamentals of Gaseous Electronics* (Wiley, New York, 1971).
[5]S. C. Brown, *Basic Data of Plasma Physics* (MIT Press, Cambridge, MA, 1966).
[6]L. B. Loeb, *Basic Processes of Gaseous Electronics* (University of California Press, Berkeley, CA, 1960).
[7]W. L. Morgan, University of Colorado, JILA Information Center Report No. 19 (1979).
[8]R. M. Thomson and A. R. Davies, Comput. Phys. Commun. **11**, 369 (1976).
[9]L. Vriens, J. Appl. Phys. **44**, 3980 (1973).
[10]F. A. S. Ligthart and R. A. J. Keijser, J. Appl. Phys. **51**, 5295 (1980).
[11]B. E. Cherrington, IEEE Trans. Electron Devices **ED-26**, 148 (1979).
[12]T. Itoh and T. Musha, J. Phys. Soc. Jpn. **15**, 1675 (1960).
[13]R. W. L. Thomas and W. R. L. Thomas, J. Phys. B **2**, 562 (1969).
[14]N. A. Tran, E. Marode, and P. C. Johnson, J. Phys. D **10**, 2317 (1977).
[15]C. Jacoboni and L. Reggiani, Rev. Mod. Phys. **55**, 645 (1983).
[16]P. E. Bauhahn, Ph.D. Dissertation, University of Michigan, 1977 (unpublished).
[17]A. D. MacDonald, *Microwave Breakdown in Gases* (Wiley, New York, 1966).
[18]P. J. Price, *Semiconductors and Semimetals*, Vol. 14, Chap. 4 (Academic, New York, 1979).
[19]M. Abromowitz and I. A. Stegun, *Handbook of Mathematical Functions* (Dover, New York, 1972).
[20]W. Fawcett, *Electronics in Crystalline Solids* (IAEA, Vienna, 1973), p. 531.
[21]P. J. Price, Solid State Electron. **21**, 9 (1978).
[22]L. J. Kieffer, *A Compilation of Electron Collision Cross Section Data for Modeling Gas Discharge Lasers*, JILA COM-74—11661, Boulder, CO (1973).
[23]L. S. Frost, Phys. Rev. **105**, 354 (1957).
[24]K. Seeger, *Semiconductor Physics* (Springer, New York, 1973).
[25]D. E. Potter, *An Introduction to Computational Physics* (Wiley, New York, 1973).
[26]P. J. Roache, *Computational Fluid Dynamics* (Hermosa, Alburquerque, NM, 1974).
[27]C. M. Lee, R. J. Lomax, and G. I. Haddad, IEEE Trans. Microwave Theory Tech. **MTT-22**, 160 (1974).
[28]P. A. Blakey, R. A. Giblin, and A. J. Seeds, IEEE Trans. Electron Devices **ED-26**, 1718 (1979).
[29]W. H. Hayt, Jr., *Engineering Electromagnetics* (McGraw-Hill, New York, 1967).
[30]J. R. East and G. I. Haddad, *GaAs FET Device Modeling and Performance*, Air Force Wright Aeronautical Laboratories, Wright Patterson Air Force Base, OH, Report Number AFWAL-TR-81-1191 (November 1981).
[31]R. Courant, K. O. Friedrichs, and H. Lewy, IBM J. Res. Develop., 215 (March 1967).
[32]C. M. Lee, Ph.D. Dissertation, University of Michigan, 1974 (unpublished).
[33]G. A. Hebner and J. T. Verdeyen, IEEE Trans. Plasma Sci. **PS-14**, 132 (1986).

[34]J. W. Coburn and E. Kay, J. Appl. Phys. **43**, 4965 (1972).
[35]K. Kohler, J. W. Coburn, D. E. Horne, E. Kay, and J. H. Keller, J. Appl. Phys. **57**, 59 (1985).
[36]O. A. Popov and V. A. Godyak, J. Appl. Phys. **57**, 53 (1985).
[37]P. Bletzinger and C. A. DeJoseph, Jr., IEEE Trans. Plasma Sci. **PS-14**, 124 (1986).
[38]C. M. Horwitz, J. Vac. Sci. Technol. **1**, 60 (1983).
[39]D. B. Graves and K. F. Jensen, IEEE Trans. Plasma Sci. **PS-14**, 78 (1986).